PROPERTIES OF ZR ALLOY CLADDING AFTER SIMULATED LOCA OXIDATION AND WATER QUENCHING

HYUN-GIL KIM*, IL-HYUN KIM, YANG-IL JUNG, JEONG-YONG PARK and YONG-HWAN JEONG
Nuclear Convergence Technology Division, Korea Atomic Energy Research Institute
1045 Daedeokdaero, Yuseong-gu, Daejeon 305-353, Korea
*Corresponding author. E-mail : hgkim@kaeri.re.kr

Received June 29, 2009
Accepted for Publication March 15, 2010

In order to study the cladding properties of zirconium after a loss-of-coolant accident (LOCA)-simulation oxidation and water quenching test, commercial Zircaloy-4 and two kinds of HANA claddings were oxidized at temperatures ranging from 900°C to 1250°C and exposed for 300 s, and then cooled to 700°C before quenching. Microstructural observations were made to evaluate the matrix characteristics with the chemical compositions after the LOCA-simulation test. Ring compression testing was then performed to compare the ductile behaviour of the HANA and Zircaloy-4 claddings. An X-ray diffraction (XRD) analysis was carried out for temperatures ranging from room temperature to 1250°C for the oxide layer to verify the oxide crystal structure at each oxidation temperature.

KEYWORDS : LOCA, Zirconium, Cladding, Zircaloy-4, HANA

1. INTRODUCTION

A loss-of-coolant accident (LOCA) is treated as one of the most important design-basis accidents in a nuclear power plant. During a LOCA, the fuel claddings are subject to high temperature oxidation and then quenched by water due to the actuation of the emergency core cooling system (ECCS) [1,2]. As a result, brittle layers of ZrO_2 and oxygen-stabilized α-Zr (α-Zr(O)) are formed on the Zr alloy cladding surface. It is known that fuel cladding loses integrity from the formation of ZrO_2 and α-Zr(O) layers since the ZrO_2 and α-Zr(O) layers are brittle [3]. Moreover, cladding ductility decreases as the oxygen concentration in the prior-β phase increases [4]. Therefore, the ductility of fuel cladding after a LOCA is gradually decreased as the thickness of these brittle layers increases, as well as with increasing oxygen concentration in the prior-β phase.

Regarding high-temperature oxidation, the oxide crystal structure is considered a very important factor to determine the oxidation kinetics of Zr cladding. It is reported that the oxidation kinetics such as the breakaway phenomenon are related to the oxide phase transformation from the monoclinic ZrO_2 to the tetragonal ZrO_2 that occur with changes in the oxidation temperature [3,5,6]. In particular, the change of oxidation kinetics at high temperatures is caused by the monoclinic/tetragonal phase transformation of ZrO_2 [6]. Thus, the particular oxide crystal structures that occur at various oxidation temperatures are considered important for the analysis of oxidation kinetics.

Presently, advanced fuel claddings in a class of materials termed high performance alloy for nuclear application (HANA) are being developed at KAERI for use with high burn-up fuel [7]. LOCA-simulation testing is required for newly developed zirconium alloy claddings such as HANA claddings, since the behaviour of fuel claddings after a LOCA is a key licensing issue. The objective of this study is to evaluate the performance of HANA claddings during a LOCA. Therefore, a comparison of the microstructure and mechanical properties of HANA and Zircaly-4 claddings under identical test conditions was made in this study. Specifically, observations of microstructural changes and a ring compression test were conducted after a LOCA-simulation test for HANA claddings, and the results were compared to those of conventional Zircaloy-4 cladding. In addition, high temperature X-ray diffraction (XRD) analysis was done to check the relationship between oxide phase transformation and oxidation kinetics for the HANA and Zircaloy-4 claddings.

2. EXPERIMENTAL PROCEDURES

Table 1 shows the chemical compositions of the HANA (HANA-5 and HANA-6) and Zircaloy-4 claddings. The outer diameter is 9.5 mm and the wall thickness is 0.57 mm in all tested claddings. To simulate a LOCA, claddings with a length of 200 mm were oxidized by steam at

Table 1. Chemical Composition of the Investigated Zirconium Alloy Claddings

Claddings	Nb	Sn	Fe	Cr	Cu	O	Zr
HANA-5	0.4	0.8	0.35	0.15	0.1	0.12	Bal.
HANA-6	1.1	-	-	-	0.05	0.12	Bal.
Zircaloy-4	-	1.5	0.2	0.1	-	0.12	Bal.

Table 2. High Temperature XRD Analysis and Oxide Thickness of Three Types of Cladding after LOCA-simulation Test

LOCA-simulation test temperature (°C)	Cladding : oxide thickness after LOCA-simulation test (μm)	XRD analysis temperature (°C)
900	HANA-5: 11 HANA-6: 11 Zircaloy-4: 11	30 900
1000	HANA-5: 18 HANA-6: 16 Zircaloy-4: 20	30 1000
1100	HANA-5: 34 HANA-6: 30 Zircaloy-4: 38	30 1100
1200	HANA-5: 56 HANA-6: 55 Zircaloy-4: 57	30 1200
1250	HANA-5: 67 HANA-6: 66 Zircaloy-4: 67	30 1250

temperatures ranging from 900°C to 1250°C for 300 s. The test time of 300 s follows that of a previous study [8]. After being oxidized in a steam environment, the oxidized claddings were cooled to the intermediate temperature of 700°C and maintained at that temperature for 100 s before being quenched in water. All claddings were oxidized on the single outer surface. A direct heating through ohmic resistance was applied to heat the cladding specimens. The temperature of the specimens was measured by using a pyrometer, which was connected to a computer to control the heating of each specimen. The accuracy of the temperature measurement using the pyrometer was affected by an intermediate medium such as a quartz chamber wall and steam flow in a chamber. To compensate, a temperature calibration was performed by using a spot-welded thermocouple on the cladding under equal environmental conditions at each temperature. Fig. 1 shows an illustration of the LOCA-simulation oxidation and water quenching scheme in this work.

The observation of cladding microstructure was performed using an optical microscope (OM) and scanning electron microscope (SEM) equipped with energy dispersive spectra (EDS) to analyze the characteristics of the ZrO_2 phase, α-Zr(O) layer and prior-β region after the LOCA-simulation test. A ring compression test was carried out to evaluate the ductility of the claddings after the LOCA-simulation test. In the ring compression test, the oxidized cladding was cut to a 10 mm length and compressed by using an Instron (Model 3366) at the loading rate of 1 mm per minute at room temperature. In the ring compression test, the sample length of 10 mm used here is shorter than the sample length of 15 mm used in the previous study [8]. The maximum load and offset strain results were averaged from three ring compression tests. The reference point of the offset strain was determined based on the load drop point where the significant load drop occurred in the strain-

stress curves in this work. Generally, ring compression tests are conducted at room temperature and at 135°C [9]; however, the test in this work was conducted at room temperature only because the Instron machine used in this study was not equipped with a heating furnace. If the test were to be performed at 135°C, the ductility of the cladding materials would be increased over that of the materials when tested at room temperature.

A microhardness test was performed by using a Knoop-type indenter (Shimadzu, Model HMV-2) to reduce the partial deviation due to microstructural differences, such as grain boundary and precipitates. The hardness for one sample is averaged from ten indentations, and the applied load is 0.1 N for 10 s. In particular, microhardness measurement was focused on the prior-β phase region since the ductility of cladding after a LOCA is considerably dependent on the property of the prior-β phase. Hydrogen uptake in the oxidized cladding was measured by a vacuum fusion method (LECO, Model RH-404). Hydrogen analysis was performed on 2-3 mm sections from the cladding samples used in the ring compression test.

The oxide phase formed on the cladding surface was analyzed using a high temperature X-ray diffractometer (Rigaku, Model D/MAX 2500H). The samples were tested at room temperature, 900°C, 1000°C, 1100°C, 1200°C and 1250°C and the heating rate was 20°C/min in a vacuum condition. The test matrix of the XRD analysis is listed in Table 2.

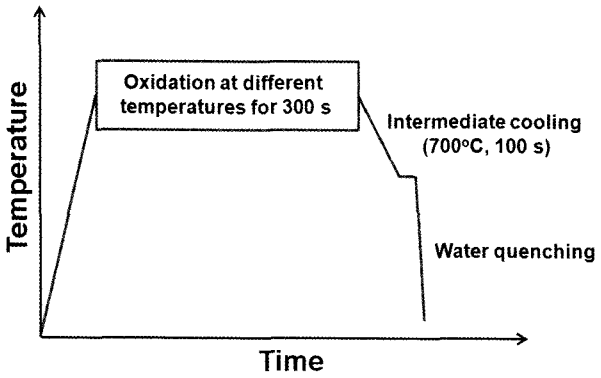

Fig. 1. Schematic Illustration of the LOCA-simulation Oxidation and Water Quenching Test

3. RESULTS AND DISCUSSION

3.1 Microstructural Characteristics

Fig. 2 is the optical micrographs of HANA-5, HANA-6 and Zircaloy-4 claddings showing the ZrO_2 phase, α-Zr(O) layer, and prior-β phase region oxidized at 1250°C for 300 s. The microstructure of the grown ZrO_2 phase was of a columnar shape in all cladding materials, whereas the microstructure of the α-Zr(O) layer and prior-β phase region differed among the three claddings. The phase characteristics between the α-Zr(O) layer and prior-β phase region were distinguished by the SEM-EDS analysis of oxygen content. Fig. 3 shows the α-Zr(O) layer and prior-β phase region of the claddings after LOCA-simulation testing at various temperatures. The morphology of the α-Zr(O) layer and prior-β phase changed with the cladding composition and oxidation temperatures. As the temperature increased, the α-Zr(O) layer grew; however, the width of the α-Zr(O) grain was decreased with increasing Nb content as well as with decreasing Sn content. Therefore, the width of the α-Zr(O) grain in HANA-6 having the highest Nb and the smallest Sn content among three claddings is less than for the other claddings.

Regarding the prior-β phase morphology of the Zircaloy-4, equiaxed grain was observed up to when the oxidation was lower than 950°C; however, a plate type structure

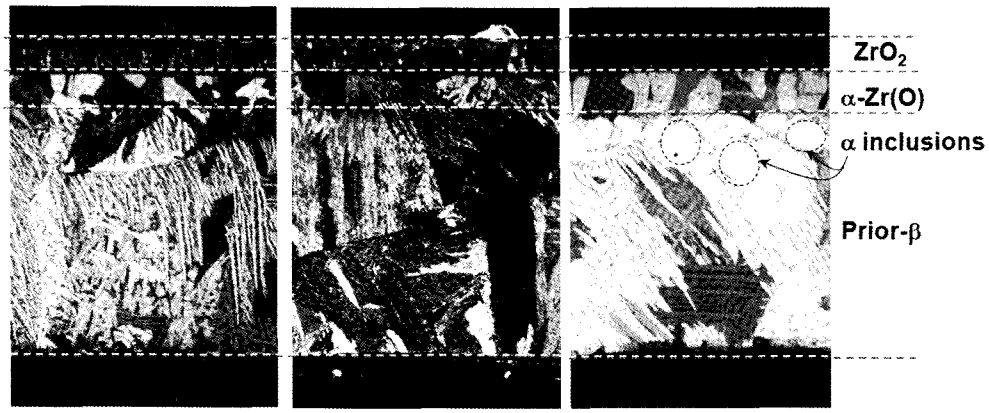

(a) HANA-5 (b) HANA-6 (c) Zircaloy-4

Fig. 2. Optical Micrographs of HANA-5, HANA-6 and Zircaloy-4 Claddings after the LOCA-simulation Test at 1250°C for 300 s

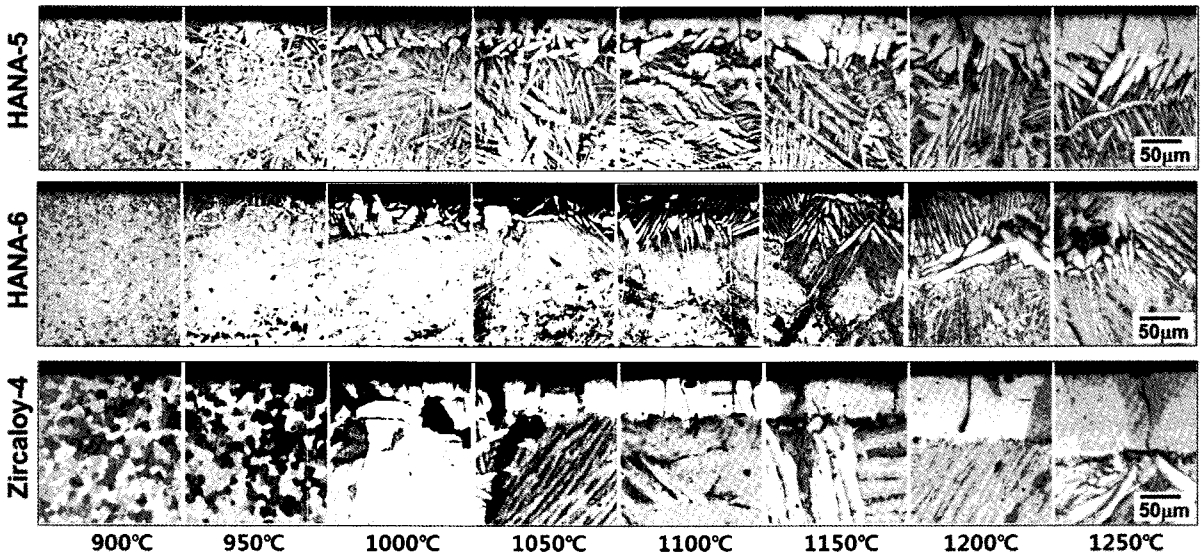

Fig. 3. Micrographs of α-Zr(O) Layer and Prior-β phase Region with the Test Temperatures and Claddings

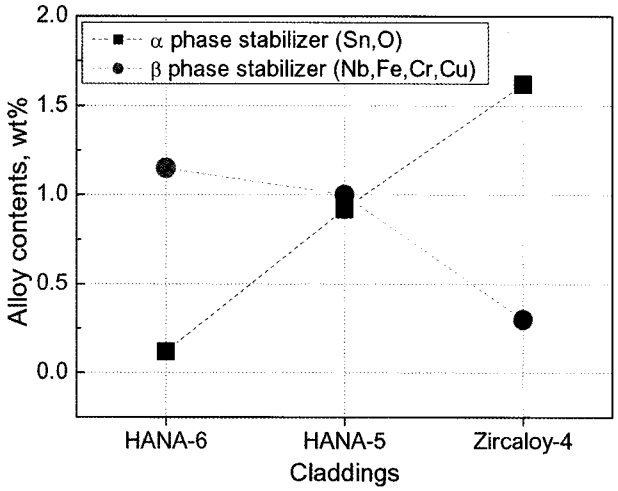

Fig. 4. Comparison of Contents between α Phase and β Phase Stabilizing Element in HANA-5, HANA-6, and Zircaloy-4 Claddings

was observed when the oxidation temperature exceeded 1000°C. The plate type structure was developed from the phase transformation of the prior-β phase by a fast cooling [10]. The microstructure change of Zircaloy-4 cladding is related to the matrix phase transformation from αZr+βZr to βZr, since the phase transformation temperature from αZr+βZr to βZr is revealed as 970°C [10]. In the HANA claddings, the plate type structure was observed at all test temperatures from 900°C to 1250°C. This means that the matrix phase transformation temperature from αZr+βZr to βZr is lower than 900°C in HANA-5 and HANA-6 claddings. Therefore, it is anticipated that the microstructural characteristics of both the α-Zr(O) layer and the prior-β phase were affected by the alloying compositions acting as an α phase stabilizer (Sn, O) and β phase stabilizer (Nb, Fe, Cr, Cu).

Fig. 4 shows a comparison of alloying element content between α phase and β phase stabilizers in the tested cladding materials. The content of α phase and β phase stabilizing elements was calculated based on the chemical composition, as shown in Table 1. This element classification between α phase and β phase stabilizers was established by Northwood's research [11]. After the LOCA-simulation oxidation and water quenching test of the three kinds of claddings, microstructural differences among the claddings could be directly related to the alloying elements in each cladding. By increasing the content of β phase stabilizing elements as well as by decreasing the content of α phase stabilizing elements in HANA-5, HANA-6 and Zircaloy-4 claddings, the widths of the α-Zr(O) and plate type structures were decreased.

3.2 Mechanical Properties

The ductility of the cladding samples after the LOCA-simulation test was evaluated by the ring compression test. Fig. 5 shows the load-displacement curves of the oxidized and water quenched HANA-5, HANA-6, and Zircaloy-4 claddings. In the ring compression test results, a significant load drop phenomenon was shown in the load-displacement curves. Such a load drop is considerably due to a fracture of brittle ZrO_2 and α-Zr(O) layers formed on the outside region of the cladding, and is also due to a decrease of ductility of the prior-β phase.

Fig. 6 shows the variation of the maximum load, and

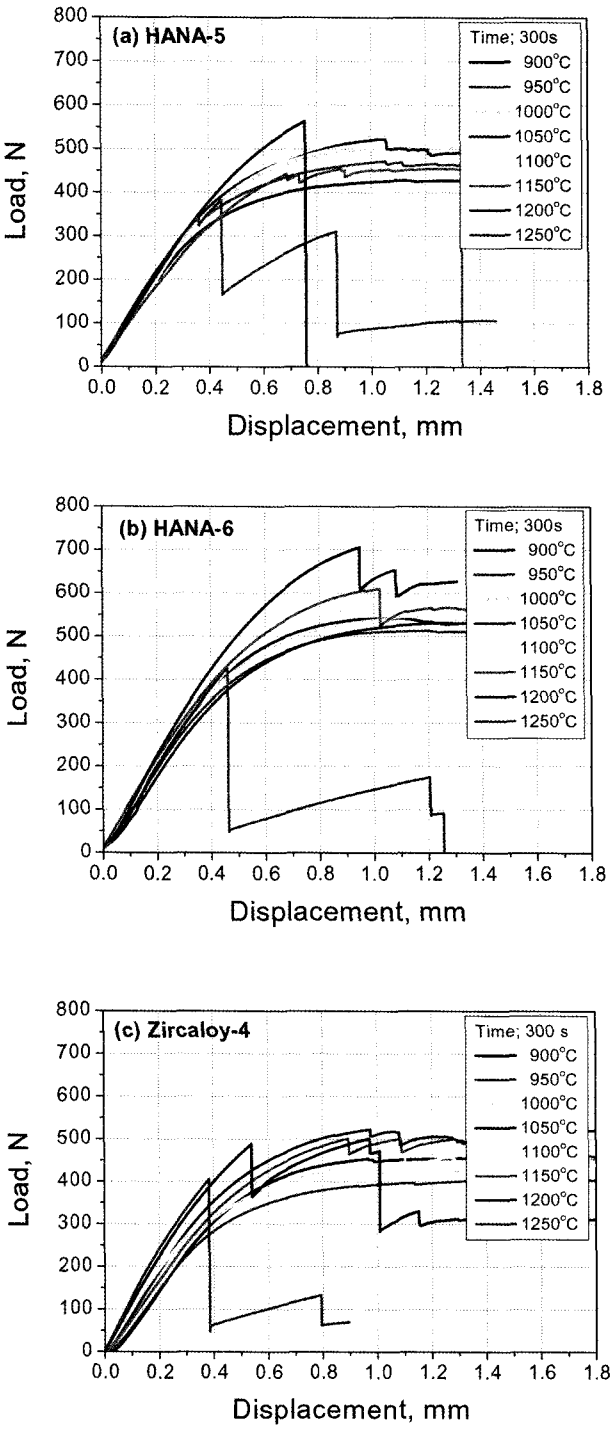

Fig. 5. Load-displacement Curve of the HANA-6 Cladding after the LOCA-simulation Test at Different Oxidized Temperatures

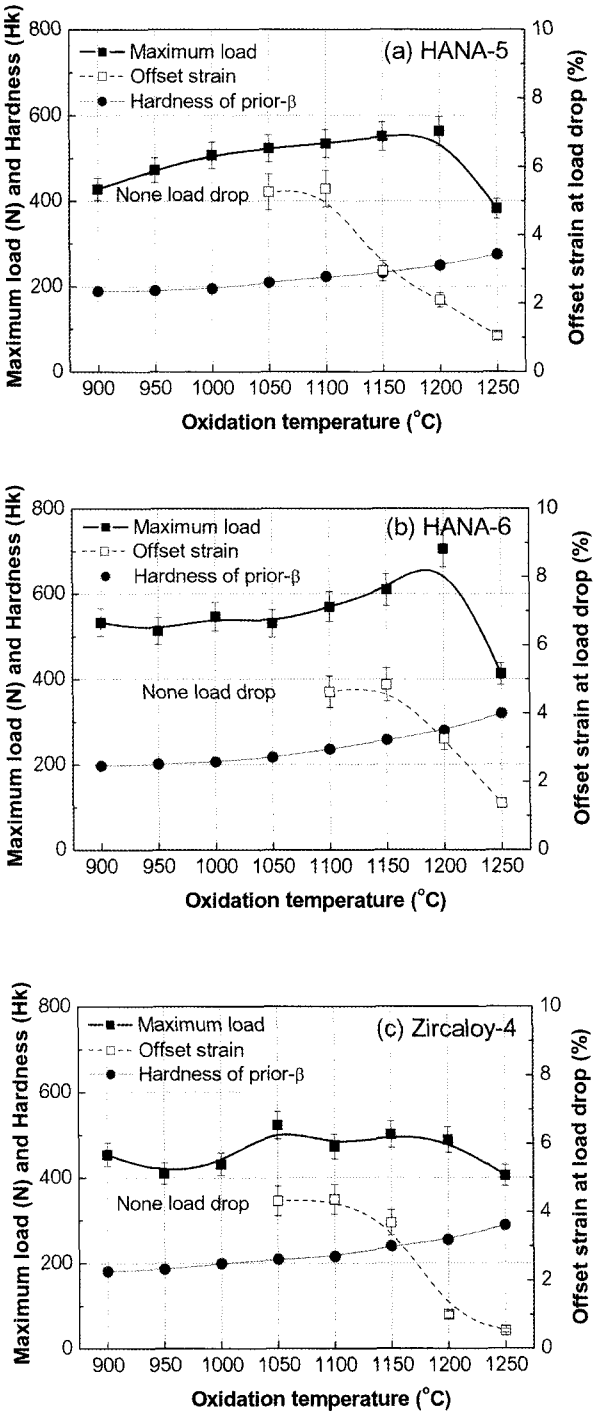

Fig. 6. Variation of Mechanical Properties of the Fuel Claddings with the Oxidation Temperatures; (a) HANA-5, (b) HANA-6, and (c) Zircaloy-4

the offset strain at the significant load drop, as well as the microhardness of the prior-β phase region according to oxidation temperature. For the Zircaloy-4 cladding, the maximum load in this study is lower than that in the previous study [8], because the sample length for the ring compression test was decreased from 15 mm to 10 mm in this study, as noted in the experimental procedures. However, the variation of the offset strain (or displacement)

at the first load drop, which decreases with increasing test temperatures, is similar in both studies. The load drop of the HANA-5, HANA-6 and Zircaloy-4 claddings was manifested at oxidation temperatures ranging from 1050°C to 1100°C. After the start of the significant load drop phenomenon, the offset strain of all the claddings was considerably decreased with increasing oxidation temperature. At oxidation temperatures exceeding 1200°C, the offset strain of the HANA-5 and HANA-6 claddings was higher than that of the Zircaloy-4 cladding. These results indicate that HANA claddings have a better ductile property than Zircaloy-4 cladding at the oxidation temperatures of 1200°C and 1250°C.

The microhardness of all tested claddings was gradually increased with increasing oxidation temperature. Although the microhardness of the HANA-6 cladding was higher than that of the HANA-5 and Zircaloy-4 claddings, the offset strain of the HANA-6 cladding was not lower than that of the HANA-5 and Zircaloy-4 claddings. As a result, it is hard to find a reasonable correlation between the ductile behavior and the microhardness of the prior β-phase.

3.3 Correlation between Microstructure and Mechanical Properties

Since the variation of the microhardness and the maximum load with oxidation temperature did not correspond with the offset strain at significant load drop as shown in Fig. 6, these two results of the hardness and maximum load could not be correlated directly to the ductility. In addition, it has been reported that the offset strain and specific energy among the offset strain, specific energy, and maximum load from ring compression test results are selected to determine the ductile-to-brittle transition [12]. Therefore, it will be necessary to find a more reasonable factor than the microhardness of the prior β-phase and the maximum load to interpret the ductility of cladding materials after a LOCA-simulation oxidation and water quenching test. To analyze the load drop behavior during the ring compression test of HANA-5, HANA-6, and Zircaloy-4 claddings, microstructural observation was made on the LOCA-simulation oxidation and water quenched claddings.

Fig. 7 shows the fractrography of the fuel claddings after the ring compression test according to oxidation temperatures. From these micrographs, the ZrO_2 and α-Zr(O) layers appear to be brittle. Thus, the ductility of the claddings after the LOCA-simulation test decreased with the increasing thickness of these two layers. Because the dimple size at the prior-β phase region decreased as the oxidation temperatures increased from 1000°C to 1200°C in all claddings, the ductility of all claddings decreased with increasing oxidation temperature.

Fig. 8 shows the total thickness of both the ZrO_2 phase and the α-Zr(O) layer formed at the cladding surface as a function of the oxidation temperature. The α-Zr(O) grains included in the prior-β phase region were excluded in calculating the α-Zr(O) layer thickness. For the irregular interface between the α-Zr(O) grains and prior-β phase of the HANA-5 and HANA-6 claddings, the middle part was taken into account in calculating the α-Zr(O) layer thickness. The thickness of the two brittle layers is considerably increased with increasing oxidation temperature in all claddings, and also it increased similarly in the three types of claddings. This means that the oxidation rate for 300 s at oxidation temperatures ranging from 900°C to 1250°C was not considerably related with the chemical composition of the cladding materials, although

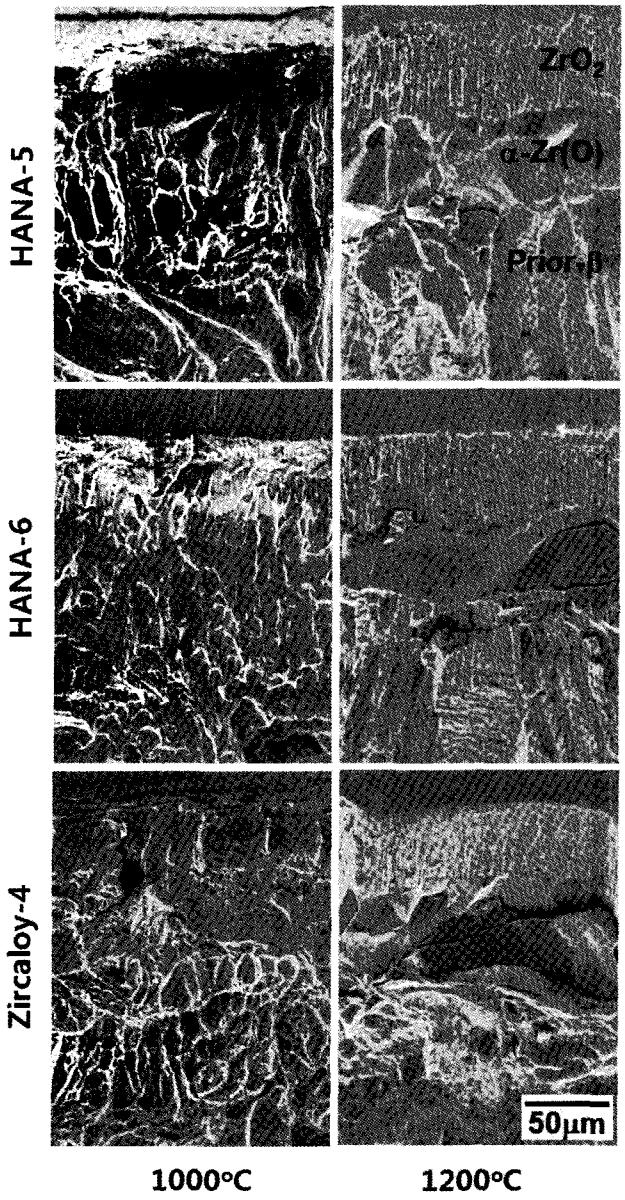

Fig. 7. Fractrography of the Fuel Claddings after Ring Compression Test with the Oxidation Temperatures

the thickness of the two layers in the HANA claddings was less than that of the Zircaloy-4 cladding at oxidation temperatures ranging from 950°C to 1100°C.

As shown in Fig. 8, the significant load drop behavior of the HANA and Zircaloy-4 claddings was manifested when the total thickness of both the ZrO_2 phase and the α-Zr(O) layer reached about 10% of the initial cladding thickness. At the high temperature region above 1200°C, the total thickness of the two brittle layers was similar in all claddings. The oxidation rate was not dependent on the alloy composition of the cladding at the very high temperatures above 1200°C. Regarding this phenomenon, the differences in oxidation behavior according to oxidation temperature would be related to the phase transformation of the ZrO_2 phase between the tetragonal structure and the monoclinic structure [5].

The oxygen content of the prior-β phase region and the offset strain at significant load drop tested at 1200°C were compared as shown in Fig. 9. The oxygen content was measured and averaged from the SEM-EDS analysis. The offset strain was decreased as the oxygen content of the prior-β phase region increased. The averaged oxygen content of the prior-β phase in this study was decreased by increasing the β phase stabilizer according to Fig. 4 and Fig. 9. The increase in oxygen content of the prior-β phase in the Zircaloy-4 cladding is caused by the formation of the α-Zr(O) inclusions in the prior-β phase region, as shown in Fig. 2. Therefore, the ductility of the HANA cladding oxidized at 1200°C is improved by the absence of the α-Zr(O) inclusions in the prior-β phase region.

The offset strain at the significant load drop was sharply decreased with the increasing thickness of the two brittle layers, as shown in Fig. 6. However, the offset strain of the HANA-5 and HANA-6 claddings was about two times as large as that of the Zircaloy-4 cladding, although the total thickness of two brittle layers of the three types of claddings was similar. This is related to the formation of the α-Zr(O) inclusions in the prior-β phase region of the Zircaloy-4 cladding, as shown in Fig. 2. Thus, the ductility decrease of the Zircaloy-4 cladding when compared to the HANA-5 and HANA-6 claddings at above 1200°C was caused by the formation of the α-Zr inclusions in the prior-β phase region. From this result, the size and volume fraction of the α-Zr(O) inclusions needs to be analyzed to understand the ductile property of cladding after LOCA-simulation testing.

Table 3 lists the hydrogen content after the LOCA-simulation test. The hydrogen contents of all claddings were lower than 31 ppm regardless of test temperatures.

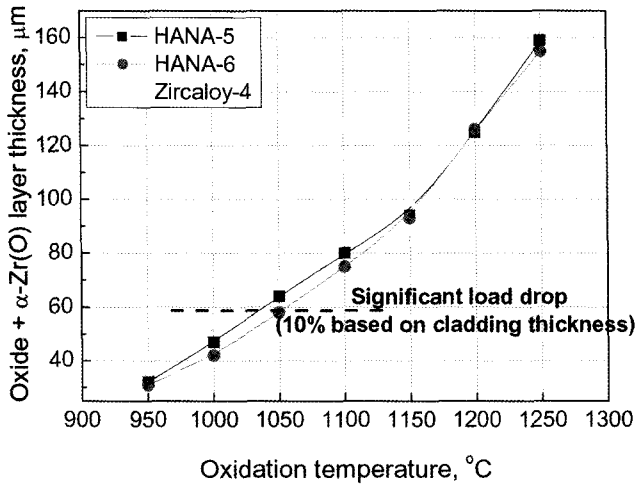

Fig. 8. Total Thickness of ZrO_2 Phase and α-Zr(O) Layer of Fuel Cladding as a Function of the Oxidation Temperature

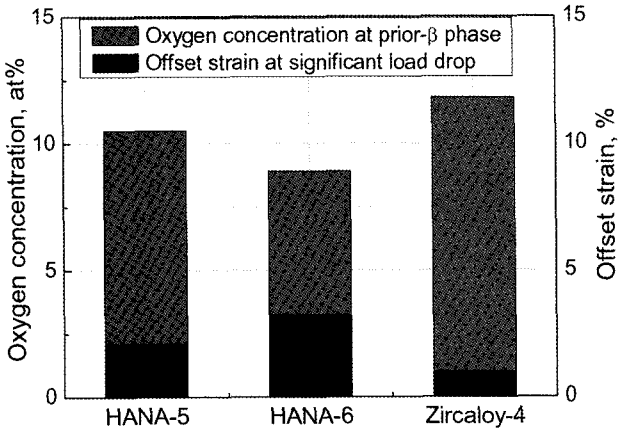

Fig. 9. Comparison between the Oxygen Concentration at Prior-β Phase and the Offset Strain at Significant Load Drop Tested at 1200°C

Table 3. Hydrogen Content of Three Types of Claddings after LOCA-simulation Test in ppm

Oxidation temperature (°C)	1000	1100	1200
HANA-5	8.0	9.0	13.0
HANA-6	16.0	12.1	10.9
Zircaloy-4	17.0	15.3	30.7

At in the previous study [8], the hydrogen uptake of the Zircaloy-4 cladding after the LOCA-simulation test is higher when compared to other results [13], but it is unclear why hydrogen uptake increased in the previous study. The hydrogen uptake during the high temperature oxidation increased considerably after the breakaway oxidation phenomenon, and the breakaway oxidation occurred when the oxidation time exceeded about 3000 s [14]. In addition, the oxide color on the oxidized surface changed from black to gray or white after the breakaway oxidation [14]. In this study, because the oxidation time is 300 s and the oxide color is maintained as black, abnormal hydrogen uptake did not occur during the LOCA-simulation test. It is therefore considered that the ductility of all claddings was unaffected by the hydrogen content in this study.

3.4 ZrO_2 Phase Effect on the Oxidation Behavior of Zr Claddings

During high temperature oxidation, the different oxidation behavior with respect to the oxidation temperature is related to the oxide phase transformation between the tetragonal phase structure and the monoclinic phase structure [5]. Further, the oxidation kinetics change from cubic to parabolic rate is attributed to the phase structure change of the oxide layer [6]. Nagase et al. proposed that the gradual change of the reaction kinetics between 900°C and 1000°C could be explained by the coexistence of the monoclinic and tetragonal phase structures in the oxide and the change of the relative proportion of the two phase structures with the temperature increase [6]. According to previous studies [5,6], the phase transformation behavior of the oxide layer is considered to be a key factor to determine the oxidation kinetics during a LOCA; however, no analysis of oxide structure has yet been performed. Therefore, high temperature X-ray was utilized here to investigate the phase transformation of the oxide layer at various temperatures.

Fig. 10 shows the crystallography of the oxide layer identified by XRD for the HANA-5, HANA-6, and Zircaloy-4 claddings. The XRD analysis was performed at 900°C, 1000°C, 1100°C, 1200°C and 1250°C in a vacuum environment to simulate the oxidation temperature during a LOCA. The XRD analysis was performed at 30°C for the claddings pre-oxidized at 900°C. The tetragonal and monoclinic phase peaks were observed for the oxides. The XRD scanning from 20° to 36° revealed the major peaks at 28.04° of 2θ corresponding to the (111) monoclinic plane and at 29.81° of 2θ corresponding to the (101) tetragonal plane, respectively. The relative intensity of the tetragonal phase can be calculated as in the following equation [15].

$$\%[ZrO_2(t)] = I(101)_t / [I(111)_m + I(-111)_m + I(101)_t] \quad (1)$$

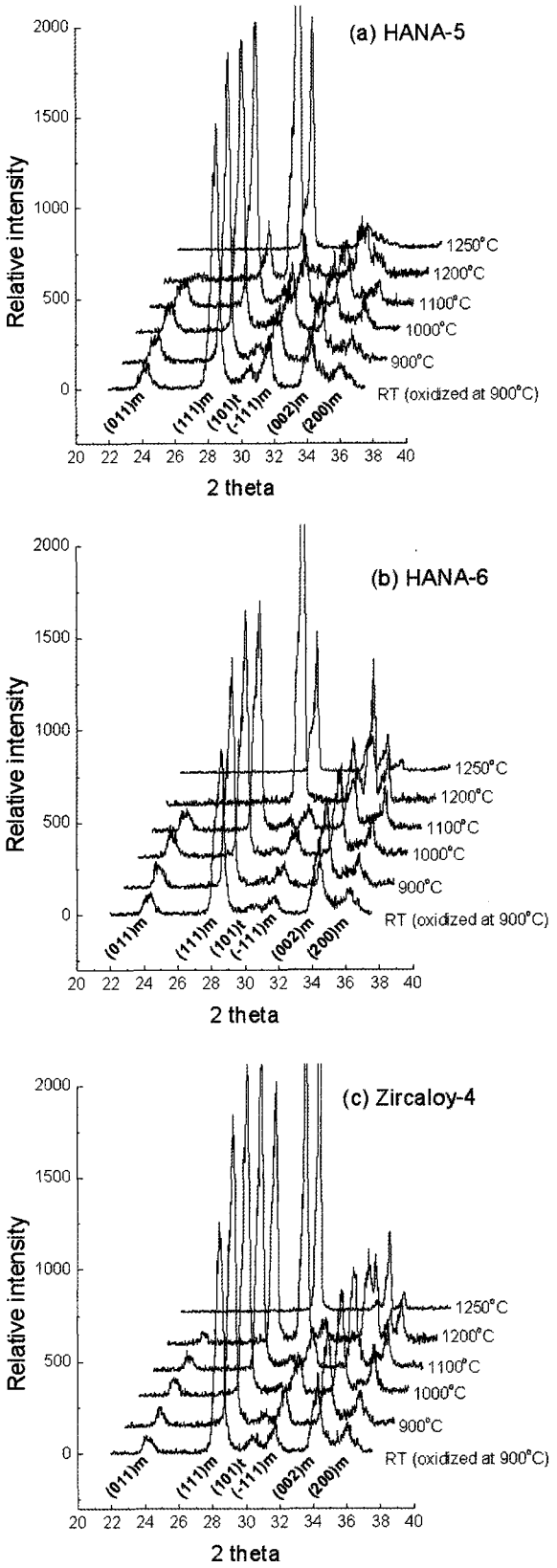

Fig. 10. Crystallography of Oxide Layer Identified by XRD for the HANA-5, HANA-6, and Zircaloy-4 Claddings with the Oxidation Temperature

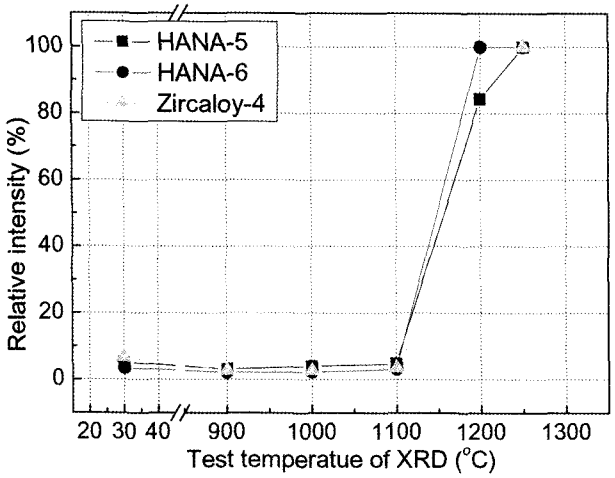

Fig. 11. Relative Intensity of (101) Tetragonal Plane of the Oxide Layer Formed on Claddings during the LOCA-Simulation Oxidation Test

Fig 11 shows the relative intensity of the (101) tetragonal plane of the oxide layer formed on claddings during the LOCA-simulation oxidation test. The intensity of the tetragonal phase was lower than 5% and was maintained up to 1100°C for all claddings. However, the relative intensity of the tetragonal phase was considerably increased at 1200°C and reached 100% at 1250°C. The change in the relative proportion of the two phase structures was observed at temperatures between 1100°C to 1250°C in all claddings. At the temperature of 1200°C, the relative intensity of the tetragonal phase was 100% in the HANA-6 oxide, 84% in the HANA-5 oxide, and 50% in the Zircaloy-4 oxide.

When compared to the oxide thickness (Table 2) and the intensity of the tetragonal phase (Fig. 11), it is suggested that the oxidation kinetics at temperatures ranging from 900°C to 1250°C were not matched to the change of the relative proportion of the monoclinic phase and tetragonal phase structures. Consequently, the oxidation kinetics during the LOCA could not be explained by the oxide phase transformation behavior of the HANA-5, HANA-6 and Zircaloy-4 claddings.

4. CONCLUSION

In order to investigate the LOCA properties of HANA-5 and HANA-6 claddings, microstructural observation, mechanical testing and XRD analysis were performed after a LOCA-simulation test. The width of α-Zr(O) and prior-β phase in the HANA-6 cladding were thinner than for other claddings. This microstructural difference was directly related to the variations between α and β phase stabilizing element contents. The load drop behavior of HANA-5, HANA-6 and Zircaloy-4 claddings was similar. However, the ductility at oxidation temperatures higher than 1200°C was higher in the HANA claddings than in the Zircaloy-4 cladding, because the α-Zr(O) inclusions were formed in the prior-β phase region of the Zircaloy-4 cladding. Although the oxide phase transformation from monoclinic to tetragonal phase was analyzed via high temperature X-ray, the oxidation kinetics during the LOCA could not be explained by the oxide phase transformation behavior in the HANA and Zircaloy-4 claddings.

ACKNOWLEDGMENTS

This study was conducted under the auspices of the Nuclear R&D program by the Ministry of Education, Science and Technology (MEST).

REFERENCES

[1] F. J. Erbacher, S. Leistikow, "Zircaloy fuel cladding behavior in a loss-of-coolant accident: a review", Zirconium in the Nuclear Industry ASTM STP **939**, 451 (1987).
[2] U. S. Code of Federal Regulations, Title 10, Energy, Parts 0 to 10, Revised January 1, 1997, U. S. Government Printing Office, Washington, DC.
[3] H. M. Chung, T. F. Kassner, "Embrittlement criteria for Zircaloy fuel cladding applicable to accident situations in Light-Water Reactors": Summary Report NUREG/CR-0344 (1980).
[4] R. E. Pawel, "Oxygen diffusion in beta Zircaloy during steam oxidation", J. Nucl. Mater. **50**, 247 (1974).
[5] J. H. Baek, K. B. Park, Y. H. Jeong, "Oxidation kinetics of Zircaloy-4 and Zr-1Nb-1Sn-0.1Fe at temperature of 700-1200°C", J. Nucl. Mater., **335**, 443 (1973)
[6] F. Nagase, T. Otomo and H. Uetsuka, "Oxidation Kinetics of Low-Sn Zircaloy-4 at the Temperature Range from 773 to 1,573 K", J. Nucl. Sci. & Tech. Vol. **40** (4), 213 (2003).
[7] Y. H. Jeong, S.Y. Park, M.H. Lee, B.K. Choi, J.H. Baek, J.Y. Park, J.H. Kim and H.G. Kim, "Out-of-pile and in-pile performance of advanced zirconium alloys (HANA) for high burn-up fuel", J. Nuclear Science and Technology, **43**, 977 (2006).
[8] J.H. Kim, M.H. Lee, B.K. Choi, Y.H. Jeong, "Failure behaviour of Zircaloy-4 cladding after oxidation and water quench", J. Nucl. Mater, **362**, 36 (2007).
[9] Y. Yan, T.A. Burtseva, M.C. Billone, "High-temperature steam-oxidation behaviour of Zr-1Nb cladding alloy E110", J. Nucl. Mater, **393**, 433 (2009).
[10] H.M. Chung, T.F. Kassner, "Pseudobinary Zircaloy-Oxygen Phase Diagram", J. Nucl. Mater., 84, 327 (1979).
[11] D. O. Northwood, D. T. Lim, "Phase transformations in zirconium and its alloys", Canadian Metallurgical Quarterly, **18**, 441 (1979).
[12] Z. Hózer, C. Györi, L. Matus, M. Horváth, J. Nucl. Mater, **373**, 415 (2008).
[13] J.-C. Brachet, V. Vandenberghe, "Comments to papers of J.H. Kim et al. [1] and M. Groβe et al. [2] recently published in JNM "On the hydrogen uptake of Zircaloy-4 and M5" alloys subjected to steam oxidation in the 1100-1250°C temperature range", J. Nucl. Mater, **395**, 169 (2009).
[14] J. H. Baek, Y. H. Jeong, "Breakaway phenomenon of Zr-

based alloys during a high-temperature oxidation", J. Nucl. Mater, **372**, 152 (2008).
[15] Ch. Valot, D. Ciosmak, M.T. Mesnier, and M. Lallemant, "Phase Analysis by Variable-Incidence X-Ray Diffraction: Application to Zirconium Oxidation", Oxidation of Metals, **48** (3/4) (1997).